

 Open access • Journal Article • DOI:10.1007/S00340-018-6980-3

Mid-infrared supercontinuum generation in fluoride fiber amplifiers: current status and future perspectives — [Source link](#)

Jean-Christophe Gauthier, Louis-Rafaël Robichaud, Vincent Fortin, Réal Vallée ...+1 more authors

Institutions: Laval University

Published on: 30 May 2018 - Applied Physics B (Springer Berlin Heidelberg)

Topics: Supercontinuum

Related papers:

- [15.2 W spectrally flat all-fiber supercontinuum laser source with >1 W power beyond 3.8 \$\mu\text{m}\$.](#)
- [High power mid-infrared supercontinuum generation in a single-mode ZBLAN fiber with up to 21.8 W average output power](#)
- [Watt-level and spectrally flat mid-infrared supercontinuum in fluoroindate fibers](#)
- [Versatile short-wave and mid-infrared sources based on wideband parametric conversion](#)
- [Midinfrared supercontinuum generation from 2 to 6 \$\mu\text{m}\$ in a silicon nanowire](#)

Share this paper:    

View more about this paper here: <https://typeset.io/papers/mid-infrared-supercontinuum-generation-in-fluoride-fiber-acp5iv6lwt>

Mid-infrared supercontinuum generation in fluoride fiber amplifiers: current status and future perspectives

Jean-Christophe Gauthier¹ · Louis-Rafaël Robichaud¹ · Vincent Fortin¹ · Réal Vallée¹ · Martin Bernier¹

¹ Centre d'optique, photonique et laser (COPL), Université Laval, Quebec G1V 0A6, Canada

Accepted for publication in *Applied Physics B* (2018) 124:122

Abstract

The quest for a compact and efficient broadband laser source able to probe the numerous fundamental molecular absorption lines in the mid-infrared (3–8 μm) for various applications has been going on for more than a decade. While robust commercial fiber-based supercontinuum (SC) systems have started to appear on the market, they still exhibit poor energy conversion into the mid-infrared (typically under 30%) and are generally not producing wavelengths exceeding 4.7 μm . Here, we present an overview of the results obtained from a novel approach to SC generation based on spectral broadening inside of an erbium-doped fluoride fiber amplifier seeded directly at 2.8 μm , allowing mid-infrared conversion efficiencies reaching up to 95% and spectral coverage approaching the transparency limit of ZrF_4 (4.2 μm) and InF_3 (5.5 μm) fibers. The general concept of the approach and the physical mechanisms involved are presented alongside the various configurations of the system to adjust the output characteristics in terms of spectral coverage and output power for different applications.

1 Introduction

An impressive amount of knowledge and new applications emerged from the widespread use of lasers in various fields of fundamental and applied research, including chemistry, biology and medicine, to name a few. This success led to a growing need for new types of laser sources as researchers and industrials are now trying to use light to solve an increasing number of problems. Due to its strong application potential in spectroscopy, the 3–8 μm spectral region known as mid-wave infrared (MWIR) has become a fertile ground for laser research over the past decade. Home to many fundamental ro-vibrational absorption lines of atmospheric pollutants such as carbon oxides (CO , CO_2), nitrogen oxides (NO_x) and hydrocarbons like methane (CH_4), which can be one to two orders of magnitude stronger than their short-wave infrared (1.4–3 μm) counterparts [1], the MWIR also happens to overlap with an atmospheric transparency window between 3 and 5 μm . While optical parametric oscillators/amplifiers (OPO/OPA) and interband cascade lasers (ICL) can provide a tunable wavelength output, namely over the whole 3–5 μm region [2, 3], applications involving hyperspectral measurements [4], multi-gas simultaneous detection [5] or identification of complex spectral signatures (i.e., standoff detection of explosives [6], early detection of cancer [7], etc.) would benefit from a broadband emission spectrum.

As opposed to thermal sources (i.e., blackbody, solar), supercontinuum (SC) sources offer both a superior brightness and a good beam quality while producing a large and relatively flat spectrum over several microns in the mid-infrared [8–10]. Originating from the spectral broadening of a seed pulse due to a wide range of nonlinear effects such as self-phase modulation (SPM) or Raman effects, SC can be generated from different pulse durations and nonlinear materials resulting in different output characteristics [11]. At present, the method for producing the broadest SC spectra is based on high energy femtosecond pulses produced by solid-state lasers (e.g., Ti: Sapphire) launched in a nonlinear medium such as crystals [12] or centimeter-long optical fibers [10, 13]. Despite the impressive spectral coverage generated, these approaches remain complex and costly, preventing them from addressing several practical applications outside of research laboratories. In contrast, fiber-based systems are much cheaper and robust, making them ideal candidates for compact application systems. While silica-based step-index [14, 15] and photonic crystal fibers (PCFs) [11] have been extensively used for SC generation, their transparency in the infrared is limited to wavelengths below 2.5 μm (~ 1 dB/m @ 2.3 μm) due to multiphonon absorption. To solve this issue, many researchers have turned themselves towards commercially available low-phonon energy materials such as fluoride glass (FG) fibers which are providing extended transparency in the mid-infrared [~ 1 dB/m @ 4.2 μm (ZrF_4) and 5.2 μm (InF_3)]. A typical approach for fiber-based SC generation consists of the multi-stage amplification of 1.55 or 2 μm nanosecond/picosecond seed pulses in doped silica fibers to reach sufficiently high peak powers to enable spectral broadening in a mechanically or fusion-spliced undoped fluoride fiber [16–18]. This master oscillator power amplifier (MOPA) technique has produced spectra up to 4.75 μm [19] as well as average output powers exceeding 21.8 W using MHz repetition rates [20] and a pulse energy of 25 μJ at 50 kHz from an all-fiber system [21]. One drawback of this technique is that a significant portion of the total SC energy (between 40 and 90%) is not converted to wavelengths beyond 3 μm mostly, because the seed wavelength remains relatively far from the targeted spectral region [22].

Recently, an approach based on the 2.8 μm amplification of picosecond seed pulses in an erbium-doped fluoride fiber amplifier was proposed as a way to obtain most of the SC energy beyond 3 μm [23]. Relying on the simultaneous interaction of optical amplification and nonlinear spectral broadening, this in-amplifier technique also provides interesting physical insights on SC generation inside of a gain media, which is still not completely understood. In this article, we will present the general concept of the in-amplifier SC generation technique and review the results obtained so far through different configurations of the system including recent efforts on power scaling and extended spectral coverage.

2 Theory and experimental setup

The in-amplifier approach (Fig. 1) is based on launching a seed pulse (Fig. 2) of desired duration and wavelength inside a doped fiber which will act both as an amplifier and as a nonlinear medium for frequency generation. To have a better control over the generated output spectrum, a segment of passive fiber can be added after the amplifier to increase the nonlinear interaction length and thus to further tailor or extend the output spectrum.

Using a doped fiber as both the amplifying and non-linear media for SC generation is not a new idea. Several studies using thulium-doped silica fibers as nonlinear media in SC experiments have shown to produce spectrally flatter and broader SC than with passive fibers, thanks to the contribution of the $^3\text{H}_4\text{-}^3\text{H}_5$ transition of thulium ions between 2.2 ~ 2.5 μm during the broadening process [24]. However, using the thulium gain around 2 μm is not efficient to generate power within the 3–5 μm region. A logical alternative was to use the 2.8 μm gain from erbium (see Fig. 3) in fluoride fibers [25]. Consequently, we designed our system to work at this wavelength, using an erbium-doped fluoride fiber seeded by 2.8 μm pulses.

The seed laser we chose to generate SC is illustrated in Fig. 2. Provided by *Light Matter Interaction Inc.*, the seed laser system used a 1064 nm passively Q-switched micro-chip laser launched in a PPLN nonlinear crystal to generate an idler around 2.8 μm through the optical parametric generation (OPG) process. A first iteration of the system provided 2 mW of average output power at a 2 kHz repetition rate, followed by a second version at 20 kHz producing 30 mW of average output power. In both cases, the system delivered ~ 400 ps pulses in a package the size of a shoe-box. Then, the pulses were launched into the fiber amplifier through a ZnSe lens ($f = 12.7$ mm) with an efficiency of about 15% at 2 kHz and 33% at 20 kHz. The ZrF₄-based glass fiber, provided by *Le Verre Fluoré*, was doped with 7 mol% of erbium. A high concentration of erbium was chosen to benefit from the maximum gain and to maximize the effect of the cooperative energy transfer ETU1. Figure 4a shows the loss spectrum of the fiber, having an impressive minimum of 2 dB/km at 2.6 μm and around 30 dB/km in the 2.8 μm gain band of erbium. The dispersion curve and mode field diameter are presented in Fig. 4b. The zero dispersion wavelength (ZDW) of the fiber (~ 1.65 μm) was calculated based on the fiber material composition and guiding properties [26]. For wavelengths beyond 4 μm , the core guiding losses are becoming increasingly important due to both the material and mode confinement losses. The 16 μm core of the fiber was surrounded by a 240–260 μm cladding with the circular symmetry broken by two parallel flats to enhance pump absorption. A fluoroacrylate polymer of lower refractive index covers the cladding to enable the multimode propagation of the pump beam at 975 nm ($\text{NA} > 0.46$). The fiber amplifier can be pumped either in co-propagation or counter-propagation, resulting in slightly different SC characteristics. When using the 2 kHz seed laser, the continuous wave (CW) fiber-coupled pump laser diode was delivering a maximum average power of 6 W at 976 nm from a 105/125 μm , 0.15 NA multimode silica fiber. This value was increased to 20 W when using the 20 kHz seed. A dichroic mirror ($R @ 980 \geq 99\%$, $T @ 2.8 \mu\text{m} \geq 90\%$) and an aspheric ZnSe lens ($f = 12.7$ mm) were used to free-space couple the 975 nm pump in the gain fiber with a launching efficiency of about 55%. After the amplifier, a section of passive fiber can be added either by stripping the pump of the doped fiber by recoating a section of the fiber with a high-index polymer (cladding mode stripper, CMS) or by adding a new fiber via fusion splicing or butt coupling. If no passive fiber was added, an endcap made of a small segment (~ 700 μm) of 220/250 μm multimode fluoride glass fiber was necessary to prevent fiber tip damage at the amplifier output due to the high peak powers. Photodegradation of the fluoride glass endcaps was not observed during our experiments after several days of operation [27]. To measure the output spectra, a scanning monochromator (Digikrom DK480) coupled to a liquid nitrogen-cooled InSb (detection up to 5.5 μm) or HgCdTe (up to 12 μm) detector was used. A broadband AR-coated germanium window (not shown) was placed at the output of the amplifier to filter out the residual signal below 1.8 μm . Finally, the average power was monitored with a low power thermopile detector (Gentec EO, XLP12-3S-H2).

3 Results

To get a better understanding of the in-amplifier technique using the erbium gain at 2.8 μm , we tested the experimental setup under different conditions, namely by changing the pumping scheme (counter-propagation vs co-propagation), the amplifier length or the seed's repetition rate and pulse energy. In the first section, we will present the evolution of the SC at different amplifier lengths for a seed repetition rate of 2 kHz in both pumping configurations. The following section will present the results obtained with an increased seed repetition rate of 20 kHz. Finally, different ways to extend the spectral coverage above the ZrF₄ transparency limit using InF₃ fibers will be discussed.

3.1 In-amplifier SC generation

3.1.1 Seed repetition rate of 2 kHz

For the first set of experiments, the seed's repetition rate was set to 2 kHz. Since the launching efficiency was of 15%, 0.3 mW (0.15 μJ) of the 2 mW (1 μJ) available was launched into the amplifier. The setup in co-propagation pumping is shown in Fig. 5. The setup was first tested with 3 amplifier lengths, namely 1, 2.4 and 5.5 m. The results are shown in Fig. 6, where we compare the SC spectra obtained with the different amplifier lengths under the same experimental conditions and illustrate the spectral evolution with respect to the increasing pump powers. The output spectrum of the OPG seed laser is appearing as the gray curve. The seed pulse spectrum, which is rather broad for a ~ 400 ps pulse, is clearly not Fourier-transform limited. This is due to the fact that parametric gain is not limited to the central idler wavelength during the OPG process. Nearby

wavelengths also experience parametric gain through non-collinear phase matching with the pump, thus leading to a broader spectrum and a beam quality and divergence degradation [28]. When the pump is turned on, amplification around 2.8 μm is first observed. Then, as the pump power is increased, the peak power of the amplified pulse becomes sufficient to enable nonlinear effects, which eventually results in the formation of a SC. Since the fiber dispersion is located well in the anomalous regime at these wavelengths, modulation instability is expected to break the pulse into many solitonic sub-components which can individually redshift through Raman soliton self-frequency shift (SSFS) [11]. This explains the strong asymmetry of the spectral broadening towards longer wavelengths.

As can be seen, a longer amplifier length improves the spectral broadening since the nonlinear interaction length is increased. Therefore, less than a watt (830 mW) of pump power was necessary with the 5.5 m amplifier to achieve a 30 mW SC spanning from 2.7 to 4.2 μm (~ 20 dB), which is broader than what was possible at 2.13 W of pump power with the 1 m amplifier length. The SC obtained with 5 m of fiber is also spectrally flatter. This can be understood considering that the great number of sub-components created from the original pulse breakup do not have the same energy, since the modulation instability pulse breakup is a noise driven process. In long fiber lengths, most of the solitonic sub-components will have enough time to redshift to different wavelengths proportionally to their energy, while in short fibers the propagation distance can be insufficient to observe this disparity, since all components can only redshift to a similar extent before reaching the end of the fiber. Finally, considering that the measured spectrum consists in an average over a very large number of slightly different individual spectra varying randomly, the resulting SC ends up looking very flat, exhibiting a spectral flatness within 3 dB over the range of 3.3–4.1 μm . The spectral broadening was limited to ~ 4.2 μm due to a combination of increasing material losses, dispersion and mode field diameter at longer wave-lengths (see Fig. 4a, b).

As mentioned earlier, our goal was to generate most of the SC energy beyond 3 μm . As can be seen in Fig. 7, an impressive total of 95% of the energy was transferred to wavelengths longer than 3 μm with the 5.5 m amplifier (green curve of Fig. 6). This is, to the best of our knowledge, the highest reported value for a fluoride fiber-based SC system (previous record of 90.6% using a Ho-doped ZBLAN fiber [29]). Even for shorter fiber lengths, the conversion ratio remains very high. This is a good illustration of the advantage of this source over systems seeding around 2 or 1.55 μm , which need significant peak powers to get enough spectral broadening to reach the MWIR region. In comparison, our system starts to generate spectral components beyond 3 μm with as little pump power as 140 mW in this case.

In the 5.5 m case, the conversion percentage starts to decrease as the pump is increased over 550 mW (yellow curve of Fig. 6, $L = 5.5$ m). This is due to an increase of the signal around 2.8 μm associated to a buildup of amplified stimulated emission (ASE), which eventually leads to parasitic lasing at the peak of the erbium gain around 2.79 μm . We believe this is due to the fact that the low power, low repetition rate seed pulses are unable to efficiently deplete the available gain at high pump powers. Hence, a growing number of excited erbium ions can decay spontaneously by emitting 2.8 μm photons that can trigger stimulated emission of other remaining excited ions, thus creating a competing signal in the amplifier. Therefore, only a very small feedback becomes necessary to enable parasitic lasing operation that eventually completely overtakes the amplification of the seed pulses. Even if the experiment was carried with 5° angle cleaves of the amplifier input and output multimode end-caps, which helped in delaying the onset of parasitic lasing, this issue prevented us from further increasing the pump power to get more output power and spectral broadening from the 5.5 and 2 m amplifiers. However, parasitic lasing was never observed at 1 m. Instead, it is the damage threshold of the endcap splice with the fluoride fiber that limited the amount of output power we could obtain with such short fiber lengths. Without an endcap, fiber tip damage caused by the very high peak powers was observed at output powers as low as 15 mW (7.5 $\mu\text{J}/\text{pulse}$). With an endcap, this damage threshold limit value for short fiber lengths was pushed up to 50 mW (25 $\mu\text{J}/\text{pulse}$, black curve of Fig. 6, $L = 1$ m). Figure 8 shows the corresponding amplification efficiency as a function of launched (Fig. 8a) and absorbed pump power (Fig. 8b) for the three amplifier lengths. An efficiency below 5% was measured, which is significantly lower than the 30% maximum efficiency of Er^{3+} : ZrF_4 CW lasers [30]. This indicates that the seed is unable to use the available gain effectively at this repetition rate.

The setup was then pumped in counter-propagation (Fig. 9) to compare the amplification efficiency and spectral broadening with co-propagation results. Amplifier lengths of 1, 2 and 5.6 m were used for the experiments. The best SC obtained for each amplifier length is shown in Fig. 10, together with the spectrum evolution of the 2 m amplifier in Fig. 11. As opposed to the co-propagating pump scheme, the broadest SC was not achieved using the longest amplifier. While the 5.6 m amplifier was able to generate new spectral components even at very low pump powers, it was also subject to parasitic lasing earlier. In this configuration, the achieved amplification efficiencies are higher than in co-propagation for every fiber length. This difference can be interpreted by looking at the gain distribution in the fiber. In counter-propagation, the highest distribution of excited erbium atoms is at the end of the fiber, where the greatest amount of pump is absorbed (3 dB/m). This means that the power of the signal is increasing together with the available gain, resulting in a better amplification efficiency. We realized through our experiments that the parasitic lasing threshold of the amplifier was very sensitive to experimental conditions, including endcap splice interface, length, and cleave angle. This, added to the fact that the pump powers were tested in discrete increments, brings some uncertainties on the parasitic lasing threshold values of the system (Fig. 12).

3.1.2 Output stability at 2 kHz

To characterize the stability of the SC signal, we measured both the average output power variation and the pulse-to-pulse variation over time. The SC source was set in the co-propagation configuration with a 5.5 m amplifier length and pumped with 0.75 W of 976 nm light, corresponding to an output power of 27.5 mW. We measured the spectrally and temporally averaged output power during 20 min, with each data point corresponding to an average over 2000 pulses (1 s) using a thermopile detector (Gentec EO, XLP12-3S-H2) linked to a data acquisition system. The result is shown in Fig. 13a. We then repeated the same measurement using this time a 10 nm bandpass filter centered around 3500 nm to get rid of the 2.8 μm residual seed source signal and focus only on newly generated spectral components (Fig. 13b). The choice of 3500 nm was based on the high spectral flatness around those wavelengths at the chosen pump power. With the 10 nm bandpass filter, the standard deviation of the measured average power increased from 0.12 to 1.35 mW. This suggests that the pulse-to-pulse variation of the spectrum is more important at longer wavelengths, which is normal for a SC generated from modulation instability.

Then, measurements were performed with an InSb and HgCdTe fast detectors coupled to an oscilloscope to measure the pulse-to-pulse power variation (Fig. 14). The pulse duration was measured at ~ 420 ps after 2 m of amplifier length [23]. Note that these two detectors had rise times

of 100 and 1 ns, respectively, so that they could not temporally resolve the ~ 400 ps pulses at $2.8 \mu\text{m}$. Both measurements were taken using the 10 nm bandpass filter centered at 3500 nm, where one pulse was measured every 30 s for a total duration of 5 min. As expected from an incoherent SC generated from noise-induced processes such as modulation instability, the output stability is far from what is typically observed with lasers. However, most applications where SC could be used do not require high pulse-to-pulse stability, since they tend to make an average over a large number of pulses.

3.1.3 Seed repetition rate of 20 kHz

To increase the output power, we replaced the 2 kHz OPG seed with a new version at a repetition rate of 20 kHz. The co-propagation setup was chosen for convenience considering that the SC output can be freely manipulated in this configuration. First, to facilitate the comparison with the 2 kHz experiments, we adjusted the seed injected power to 3 mW, which corresponds to the same pulse energy but with a 10 fold increase of the number of pulses for a given time interval. Due to availability, we did not use the exact same fiber lengths than for the 2 kHz experiments, replacing lengths of 1, 2.4 and 5.5 m with 1, 2.7 and 5.8 m, respectively. The SC spectra were measured following the same procedure than in the 2 kHz experiments. Figure 15 shows the SC spectra for the three fiber amplifier lengths operated under identical pumping and seeding conditions. As expected, a longer fiber resulted in a broader spectrum and a higher average output power due to the increased nonlinear interaction length and available gain, respectively.

When compared to the 2 kHz experiment, the results at 20 kHz show a much higher amplification efficiency, moving from $\sim 5\%$ up to 23.1% with respect to absorbed pump power (Fig. 16a). This confirms that a repetition rate of 2 kHz was too slow to efficiently extract the available gain, leaving the erbium population inversion remains undepleted for hundreds of microseconds between pulses. When increased to 20 kHz, seed pulses were able to depopulate the ${}^4I_{11/2}$ level more frequently, thus resulting in higher amplification efficiencies. In Fig. 16b, the trend surprisingly suggests that the parasitic lasing threshold occurs at lower pump powers when the amplifier is seeded at 20 kHz. However, it is worth mentioning that the step between 1.1 and 0.83 W of pump power only represents a single increment of pump diode current in our experimental protocol. Since the parasitic lasing threshold of the amplifier is very sensitive to experimental conditions, we believe that the parasitic lasing threshold was mostly unaffected by the increased repetition rate. This would mean that even at 20 kHz, the population inversion is able to stay undepleted for long enough to create an ASE buildup leading to parasitic lasing inside of the amplifier.

To achieve the best performances from our 20 kHz setup, we increased the launched OPG seed power to 10 mW, which corresponds to the maximum we could get from our system (30 mW output with 33% launching efficiency). The best SCs measured for amplifier lengths of 2.7, 4 and 5.8 m are shown in Fig. 17. Since 1 m long amplifiers do not produce very broad spectra, we decided to test a 4 m amplifier, which gave us the highest output power (485 mW) and a spectral coverage up to $4 \mu\text{m}$ (-20 dB level). However, the 5.8 m amplifier produced the broadest (up to $4.2 \mu\text{m}$) and most flat (1 dB between 3.1 and $3.85 \mu\text{m}$) SC with 344 mW of average output power. The fraction of SC energy beyond $3 \mu\text{m}$ for the three fiber lengths were of 32% (2.7 m), 82% (4 m) and 72% (5.8 m). Compared to the 3 mW seed results, it is interesting to note that the output power efficiencies (with respect to launched pump power) are almost 5% higher with the 10 mW seed, as shown in Fig. 18a. However, trying to further increase the seed power would not translate into a linear amelioration of the efficiency, since we are already getting relatively close to the theoretical Stokes efficiency limit of $\sim 30\%$ [25].

From Fig. 18b, it appears that changing the seed power from 3 to 10 mW also improved (raised) the parasitic laser threshold of the amplifier by a factor of 1.6–1.9 depending on the fiber length. However, since the experimental parasitic thresholds can be very sensitive to external factors, the comparison between the same fiber lengths (with identical experimental conditions) should be considered as the most important information.

3.2 Extending the spectral coverage using fluoroindate fibers

For a wide range of applications, especially in spectroscopy and remote sensing, broadband laser radiation covering the whole $3\text{--}5 \mu\text{m}$ spectral range could be of great interest. Notably, many atmospheric pollutants possess strong absorption bands at wavelengths longer than $4 \mu\text{m}$, such as CO ($4.5\text{--}4.9 \mu\text{m}$), CO₂ ($4.2 \mu\text{m}$), SO₂ ($4 \mu\text{m}$) and N₂O ($\sim 4.0 \mu\text{m}$ and $4.5 \mu\text{m}$). To extend the SC spectral coverage to $5 \mu\text{m}$ inside an optical fiber, different options are presented in Fig. 19. We selected fluoroindate glass fibers (InF₃) considering the extra $1 \mu\text{m}$ transparency extent between 4 and $5 \mu\text{m}$ as compared to fluoro-zirconate (e.g., ZBLAN) glass fibers and its chemical compatibility with ZrF₄-based fibers which greatly facilitates the splicing process.

3.2.1 Cascaded SC generation in an InF₃ fiber at 2 kHz

Our initial experiments were performed with the 2 kHz OPG seed. The experimental setup is depicted in Fig. 20. The InF₃ fiber (shown in Fig. 21) was provided by Le Verre Fluoré and had a $100 \mu\text{m}$ diameter cladding and an average core diameter size of $13.5 \mu\text{m}$ (increasing from 12.5 to $14.5 \mu\text{m}$ along the 31 m fiber length). With a NA of 0.3, it was slightly multimode (average cut-off wavelength of $\sim 5.3 \mu\text{m}$) and had impressively low minimal losses of 12 dB/km at $3.8 \mu\text{m}$. The InF₃ fiber was fusion spliced to a short length (1.25 m) of the previously introduced Erdoped fluoride glass fiber so that most of the spectral broadening would occur inside of the InF₃ fiber. Fluoroindate fiber lengths of 1, 15 and 31 m were tested, with the results shown in Fig. 22. The SC obtained with 31 m is not presented to avoid redundancy with the very similar 15 m experiment. In fact, the additional 16 m of fiber slightly reduced the output power due to the extra losses and did not produce significant extra spectral broadening.

Even at low pump powers (a few 100 mW), a significant spectral broadening is generated, with the resulting SC reaching almost $5 \mu\text{m}$ after only 1 m of InF₃ fiber. With 15 m of fiber, the SC extends over more than one octave from 2.4 to $5.4 \mu\text{m}$ (-20 dB level), with 82% of its energy

beyond 3 μm . More details about the experimental procedure and results can be found in [31]. At first glance, one can also see that the spectra are much less flat compared to previous experiments without InF_3 , with the apparition of a curious peak at 4.2 μm that particularly stands out. A possible explanation for this comes from the multimode nature of the InF_3 fiber. Given that we are using long picosecond pulses for our experiment, the higher-order modes are expected to be efficiently excited and contain part of the SC energy [32]. In our case, both the LP01 and LP11 modes exist at wavelengths higher than 3.5 μm . It is believed that the peak at 4.2 μm could be caused by a second zero dispersion wavelength seen by the solitons propagating in the LP11 mode, resulting in a “spectral recoil”, or a halt of their self-frequency shift around this wavelength. If this is the case, it would lead to a significant part of the SC energy accumulating near the second ZDW, creating the aforementioned peak, and to an increased energy transfer to phase-matched dispersive waves as proposed in [33, 34]. To experimentally gain more insight about this behavior, we repeated the experiment with another InF_3 fiber having the same glass composition but a smaller core diameter of 11–12 μm along the fiber length, which should result in a displacement of the second ZDW of the LP11 mode and therefore of the 4.2 μm peak.

3.2.2 Cascaded InF_3 at 20 kHz with a 10 μm core

For this second experiment we used the same setup configuration, except that the 2 kHz seed was replaced with the one operating at 20 kHz. The fusion splice made between the amplifier and the 14 m InF_3 fiber segment also had about 20% losses. A 2.8 μm seed power of 7 mW was launched into the amplifier. The SC spectrum is shown in Fig. 23 and compared to the previous result at 2 kHz.

Apart from the peak now located around ~ 3.6 μm , the 145 mW SC looks similar in shape as what was obtained using the first InF_3 fiber. In both cases, the parasitic lasing threshold limited the maximum achievable output power. It is believed that the fusion splice between the amplifier and the InF_3 fiber may cause some feedback at the interface, explaining why the threshold is reached at relatively low pump powers for a 1.25 m amplifier. Unfortunately, we do not have access to an experimental dispersion curve for the InF_3 fibers to verify our explanation of the two strong peaks. On the other hand, we had access to the chemical composition (same for both fibers), allowing us to model a dispersion curve for the LP01 and LP11 modes from the Sellmeier coefficients [26]. Since our fibers did not have a constant core size, the curves presented in Fig. 24 were computed for several scenarios including the boundary values of each core size range.

For the 2 kHz experiment (12.5–14.5 μm core diameter fiber) the peak was located near 4.2 μm and the 2nd ZDW calculated value for cores of 12.5 and 13 μm is between 4.0 and 4.3 μm . For the 11–12 μm core diameter fiber, the experimental peak was centered at 3.6 μm while we obtained a 2nd ZDW calculated value between 3.3 and 3.8 μm for 11 and 12 μm core. Hence, our simulation seems to confirm our hypothesis since the computed 2nd ZDWs of the LP11 mode fit well with the observed wavelengths of the two observed strong peaks in the output spectra (Fig. 23).

4 Final discussion on practical considerations

An overview of previously reported fiber-based MWIR SC sources using fluoride glass is presented in Table 1. While MOPA systems based on 1.55 or 2 μm amplification have proven to be robust systems able to generate high average powers and a broad spectrum, the production of high SC pulse energy beyond 3 μm , which is important to many remote sensing applications, remains a challenge. To the best of our knowledge, the highest SC energy fraction beyond 3 μm for a 1.55 μm MOPA system using a passive ZBLAN fiber is of 61% [35]. However, the system produced pulse energies of only 3.2 μJ . A pulse energy of 25 μJ was obtained by Yang et al. at 50 kHz, but the SC had only 27.4% of its energy beyond 2.5 μm . Interestingly, a SC energy fraction beyond 3 μm of 90.6% was demonstrated recently with a 1.55 μm MOPA seed source launched into an holmium-doped ZBLAN fiber amplifier [29]. While several preliminary spectral broadening steps were necessary to reach the holmium gain band at 2.9 μm , the spectral broadening inside the amplifier was very asymmetrical towards the longer wavelengths and generated a very flat spectrum (3 dB from 2.9 to 3.7 μm), thus showing another example of the advantage of using in-amplifier techniques far in the anomalous dispersion regime. Nonetheless, the output of the source was of only 8.2 μJ (411 mW at 50 kHz). With our approach, we managed to obtain 24 μJ with 82% of this energy beyond 3 μm (4 m amplifier, 20 kHz, 485 mW) and almost 40 μJ (82% beyond 3 μm) when using the setup in counter-propagation at 2 kHz [23].

Also, using a single fiber amplifier is beneficial to the global energy efficiency of the system. Since each amplification stage have its respective amplification efficiency and sometimes need a dedicated pump source, the total power efficiency of the system tends to decrease with complexity. In our case, the electrical consumption of the whole laser system was measured to be 100 W when the OPG seed was operated at its maximum power. This value increased to 120 W when the 976 nm pump was turned on and set to 2.35 W of optical power, which was the maximal value used in our experiments. The total energy consumption of the source thus represents roughly the same electrical power needed for two standard incandescent light bulbs. Moreover, we demonstrated that only 1 W or lower of pump power from a standard 976 nm diode was sufficient to produce a broad output spectrum, extending over the whole 3–5 μm region.

Options to improve the system include moving to an all-fiber design, which would improve the overall ruggedness and reliability of the source. We believe this could also lead to better performances by eliminating possible free-space reflections contributing to the parasitic lasing threshold, which is the main limiting factor for power scaling. Efforts are currently under way to address this problem. Finally, we are confident that we could get a similar spectral flatness over the 3–5.5 μm range than with the 5.8 m amplifier at 20 kHz (1 dB between 3.1 and 3.85 μm) given the availability of an erbium-doped InF_3 fiber single-mode over the entire SC spectral region. This would also lead to a significant decrease in the system complexity.

5 Conclusion

In this paper, we reviewed our recent progress on in-amplifier SC generation in the mid-infrared based on erbium-doped fluoride fibers. We investigated the effect of fiber length, pumping configuration, seed repetition rate and power on the SC output emphasizing the different challenges and limiting factors of the technique. Spectrally flat SCs were demonstrated with up to 95% of their energy beyond 3 μm and spectral coverage reaching 4.2 μm in erbium-doped fluoride fibers and 5.5 μm in InF_3 . At 2 kHz, a SC with 48 mW (co-propagation) and 77 mW (counter-propagation) of average output power were achieved, corresponding to a pulse energy of 24 and 38.5 μJ . Using the 20 kHz seed repetition rate, the average power increased to 485 mW (co-propagation) and moved from 8 to 145 mW in InF_3 fibers. By further increasing the repetition rate of the seed or by delaying the onset of parasitic lasing, a watt-level output power should be within reach. Recently, a SC extending up to 8 μm was reported with a similar approach using a cascaded As_2Se_3 step-index chalcogenide fiber [40]. It is worth mentioning that this technique is not limited to erbium-doped fluoride fibers but could be adapted to different types of dopants and/or glass hosts with the right pumping scheme. In another study, we also showed that this concept is not even limited to SC generation, as it can be applied to create high-power tunable solitons when seeded with femtosecond pulses coming from a mode-locked 2.8 μm fiber laser [41]. In light of these numerous possibilities, we hope this approach to in-amplifier SC generation in the mid-infrared helps opens new application opportunities and research ideas.

Acknowledgements

The authors thank the Natural Sciences and Engineering Research Council of Canada (NSERC), the Canadian Foundation for Innovation (CFI) (Grant no. 5180), and the Fonds de Recherche du Québec—Nature et Technologies (FRQNT) (Grant no. 144616). We also thank Darren Kraemer from *Light Matter Interaction inc.* for helpful discussions and *Le Verre Fluoré* for providing the InF_3 fibers. Funding was provided by Canadian Network for Research and Innovation in Machining Technology, Natural Sciences and Engineering Research Council of Canada (Grant no. IRCPJ469414-13).

References

- [1] I.E. Gordon, L.S. Rothman, Y. Babikov, A. Barbe, D. Chris Benner, P.F. Bernath, M. Birk, L. Bizzocchi, V. Boudon, L.R. Brown, A. Campargue, K. Chance, E.A. Cohen, L.H. Coudert, V.M. Devi, B.J. Drouin, A. Fayt, J.M. Flaud, R.R. Gamache, J.J. Harrison, J.M. Hartmann, C. Hill, J.T. Hodges, D. Jacquemart, A. Jolly, J. Lamouroux, R.J. Le Roy, G. Li, D.A. Long, O.M. Lyulin, C.J. Mackie, S.T. Massie, S. Mikhailenko, H.S.P. Müller, O.V. Naumenko, A.V. Nikitin, J. Orphal, V. Perevalov, A. Perrin, E.R. Polovtseva, C. Richard, M.A.H. Smith, E. Starikova, K. Sung, S. Tashkun, J. Tennyson, G.C. Toon, V.G. Tyuterev, G. Wagner, *J. Quant. Spectrosc. Radiat. Transf.* 203, 3 (2017)
- [2] T. Steinle, A. Steinmann, R. Hegenbarth, H. Giessen, *Opt. Express* 22, 9567 (2014)
- [3] I. Vurgaftman, R. Weih, M. Kamp, J.R. Meyer, C.L. Canedy, C.S. Kim, M. Kim, W.W. Bewley, C.D. Merritt, J. Abell, S. Höfling, *J. Phys. D Appl. Phys.* 48, 123001 (2015)
- [4] Z. Wang, C. Li, M. Zhou, H. Zhang, W. He, W. Li, Y. Qiu, *Proc. SPIE Int. Soc. Opt. Eng.* 10156, 101560I (2016). <https://doi.org/10.1117/12.2244778>
- [5] N. Cezard, A. Dobroc, G. Canat, M. Duhant, W. Renard, C. Alhenc-Gelas, S. Lefebvre, J. Fade, *Proc. SPIE Int. Soc. Opt. Eng.* 8182, 81820V, (2011)
- [6] M. Kumar, M.N. Islam, F.L. Terry, M.J. Freeman, A. Chan, M. Neelakandan, T. Manzur, *Appl. Opt.* 51, 2794 (2012)
- [7] A.B. Seddon, *Phys. Status Solidi Basic Res.* 250, 1020 (2013)
- [8] M. Michalska, J. Mikolajczyk, J. Wojtas, J. Swiderski, *Sci. Rep.* 6, 1 (2016)
- [9] G. Qin, X. Yan, C. Kito, M. Liao, C. Chaudhari, T. Suzuki, Y. Ohishi, *Appl. Phys. Lett.* 95, 1 (2009)
- [10] C.R. Petersen, U. Møller, I. Kubat, B. Zhou, S. Dupont, J. Ramsay, T. Benson, S. Sujecki, N. Abdel-Moneim, Z. Tang, D. Furniss, A. Seddon, O. Bang, *Nat. Photonics* 8, 830 (2014)
- [11] J.M. Dudley, G. Genty, S. Coen, *Rev. Mod. Phys.* 78, 1135 (2006)
- [12] J.J. Pigeon, S.Y. Tochitsky, C. Gong, C. Joshi, *Opt. Lett.* 39, 3246 (2014)
- [13] T. Cheng, K. Nagasaka, T.H. Tuan, X. Xue, M. Matsumoto, H. Tezuka, T. Suzuki, Y. Ohishi, *Opt. Lett.* 41, 2117 (2016)
- [14] C. Xia, M. Kumar, M.Y. Cheng, O.P. Kulkarni, M.N. Islam, A. Galvanauskas, F.L. Terry, M.J. Freeman, D.A. Nolan, W.A. Wood, *IEEE J. Sel. Top. Quantum Electron.* 13, 789 (2007)
- [15] M. Tao, T. Yu, Z. Wang, H. Chen, Y. Shen, G. Feng, X. Ye, *Sci. Rep.* 6, 2 (2016)
- [16] V.V. Alexander, O.P. Kulkarni, M. Kumar, C. Xia, M.N. Islam, F.L. Terry, M.J. Welsh, K. Ke, M.J. Freeman, M. Neelakandan, A. Chan, *Opt. Fiber Technol.* 18, 349 (2012)
- [17] K. Yin, B. Zhang, L. Yang, J. Hou, *Opt. Lett.* 42, 2334–2337 (2017)
- [18] A.M. Heidt, J.H.V. Price, C. Baskiotis, J.S. Feehan, Z. Li, S.U. Alam, D.J. Richardson, *Opt. Express* 21, 24281 (2013)

- [19] P. Moselund, C. Petersen, L. Leick, J. Seidelin Dam, P. Tidemand-Lichtenberg, C. Pedersen, Adv. Solid-State Lasers Congr. (2013). JTh5A.9
- [20] K. Liu, J. Liu, H. Shi, F. Tan, P. Wang, Opt. Express 22, 24384 (2014)
- [21] W.-Q. Yang, B. Zhang, J. Hou, K. Yin, Z.-J. Liu, Chin. Phys. B 23, 054208 (2014)
- [22] J. Swiderski, Prog. Quantum Electron. 38, 189 (2014)
- [23] J.-C. Gauthier, V. Fortin, S. Duval, R. Vallée, M. Bernier, Opt. Lett. 40, 5247 (2015)
- [24] J. Geng, Q. Wang, S. Jiang, Appl. Opt. 51, 834 (2012)
- [25] M. Pollnau, S.D. Jackson, IEEE J. Sel. Top. Quantum Electron. 7, 30 (2001)
- [26] L. Zhang, F. Gan, P. Wang, Appl. Opt. 33, 50 (1994)
- [27] N. Caron, M. Bernier, D. Faucher, R. Vallée, Opt. Express 20, 22188 (2012)
- [28] Y. Guan, J.W. Haus, P. Powers, J. Opt. Soc. Am. B 21, 1225 (2004)
- [29] L. Yang, B. Zhang, K. Yin, T. Wu, Y. Zhao, J. Hou, Photon. Res. 6, 417–421 (2018)
- [30] D. Faucher, M. Bernier, G. Androz, N. Caron, R. Vallée, Opt. Lett. 36, 1104 (2011)
- [31] J.-C. Gauthier, V. Fortin, J.-Y. Carrée, S. Poulain, M. Poulain, R. Vallée, M. Bernier, Opt. Lett. 41, 1756 (2016)
- [32] I. Kubat, O. Bang, Opt. Express 24, 2513 (2016)
- [33] C.R. Petersen, P.M. Moselund, C. Petersen, U. Møller, O. Bang, Opt. Express 24, 749 (2016)
- [34] P. Falk, M.H. Frosz, O. Bang, L. Thrane, P.E. Andersen, A.O. Bjarklev, K.P. Hansen, J. Broeng, Opt. Lett. 33, 621 (2008)
- [35] J. Swiderski, M. Michalska, Opt. Lett. 39, 910–913 (2014)
- [36] S. Liang, L. Xu, Q. Fu, Y. Jung, D.P. Shepherd, D.J. Richardson, S.-U. Alam, Opt. Express 26, 6490 (2018)
- [37] M. Michalska, P. Grzes, P. Hlubina, J. Swiderski, Laser Phys. Lett. 15, 045101 (2018)
- [38] J. Swiderski, F. Theberge, M. Michalska, P. Mathieu, D. Vincent, Laser Phys. Lett. 11, 15106 (2014)
- [39] M. Michalska, J. Mikolajczyk, J. Wojtas, J. Swiderski, Sci. Rep. 6, 39138 (2016)
- [40] L.-R. Robichaud, V. Fortin, J.-C. Gauthier, S. Châtigny, J.-F. Couillard, J.-L. Delarosbil, R. Vallée, M. Bernier, Opt. Lett. 41, 4605 (2016)
- [41] S. Duval, J. Gauthier, L.-R. Robichaud, P. Paradis, M. Olivier, V. Fortin, M. Bernier, M. Piché, R. Vallée, Opt. Lett. 41, 5294 (2016)

Table 1 Overview of mid-infrared SC obtained with fiber-based systems using fluoride glasses

Architecture	Rep. rate	Type of fiber	Spectrum (μm)	Avg. power (W)	Pulse energy (μJ)	Refs.
1.55 μm MOPA + TDFA (1 ns)	6 MHz	ZBLAN	1.9–4.2	15.2	2.5	[17]
2 μm gain-switch (33 ps)	1 MHz	ZBLAN	0.75–4	1.1	1.1	[18]
1.55 μm MOPA + TDFA (3 ns)	350 kHz	ZBLAN	1.75–4.75	1.2	3.5	[19]
2 μm MOPA (24 ps)	93.6 MHz	ZBLAN	1.9–3.8	21.8	0.25	[20]
1.57 + 2 μm MOPA (2 ns)	50 kHz	ZBLAN	1.8–4.3	1.24	25	[21]
1.55 μm MOPA (1 ns)	700 kHz	ZBLAN	0.85–4.2	2.24	3.2	[35]
1.55 μm MOPA (1.6 ns)	50 kHz	Ho: ZBLAN	2.8–3.9	0.411	8.2	[29]
2.8 μm amplified OPG (400 ps)	2 kHz	Er: ZBLAN	2.6–4.1	0.08	38.5	[23]
2.8 μm amplified OPG (400 ps)	20 kHz	Er: ZBLAN	2.7–4.1	0.485	24	This Work
2 μm MOPA (35 ps)	1 MHz	InF3	0.75–5	1.76	1.8	[36]
1.55 μm MOPA (1 ns)	500 kHz	InF3	1.85–4.1	1.4	2.8	[37]
1.55 μm MOPA (1 ns)	420 kHz	InF3	1–3.05	2.09	5	[38]
Tunable OPG (70 ps)	1 kHz	InF3	1.9–5.3	0.008	8	[39]
2.8 μm amplified OPG (400 ps)	2 kHz	Er: ZBLAN + InF3	2.4–5.4	0.008	4	[31]
2.8 μm amplified OPG (400 ps)	20 kHz	Er: ZBLAN + InF3	2.6–5.4	0.145	7	This Work

A more comprehensive review of SC in soft glasses can be found in [22]

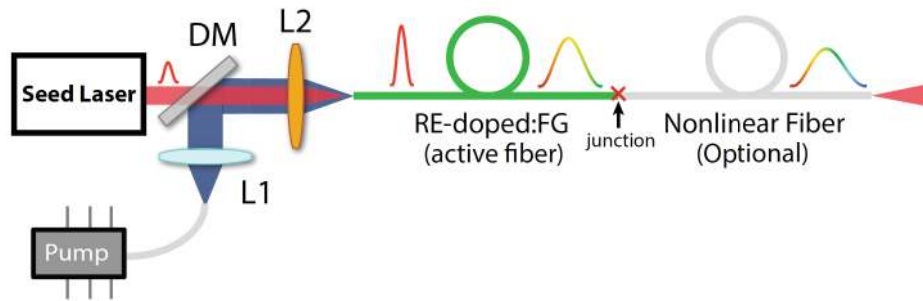


Fig. 1 Typical setting of the *in-amplifier* experimental setup in the co-propagation pumping scheme. A seed pulse is amplified in a rare-earth doped fluoride glass fiber pumped by a laser diode. New spectral components are generated during the amplification process inside

the gain fiber. A passive nonlinear fiber (e.g., ZrF_4 , InF_3 , or chalcogenide) can be added to extend the spectral coverage. *DM* dichroic mirror; *L1* silica lens; *L2* ZnSe lens; *Junction* fusion splice/lens coupling/cladding mode stripper

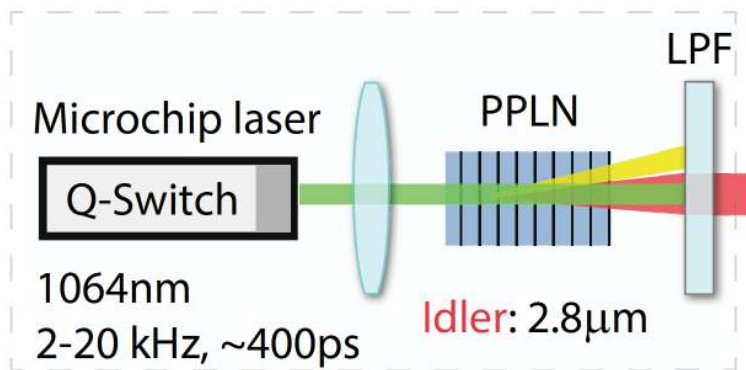


Fig. 2 Schematic of the 2.75 μ m Optical Parametric Generation (OPG) source producing the initial picosecond seed pulses. The periodically poled lithium niobate (PPLN) crystal converts part of the 1064 nm signal to 2.75 μ m which is transmitted through the Long-Pass Filter (LPF) and launched into the fluoride fiber amplifier

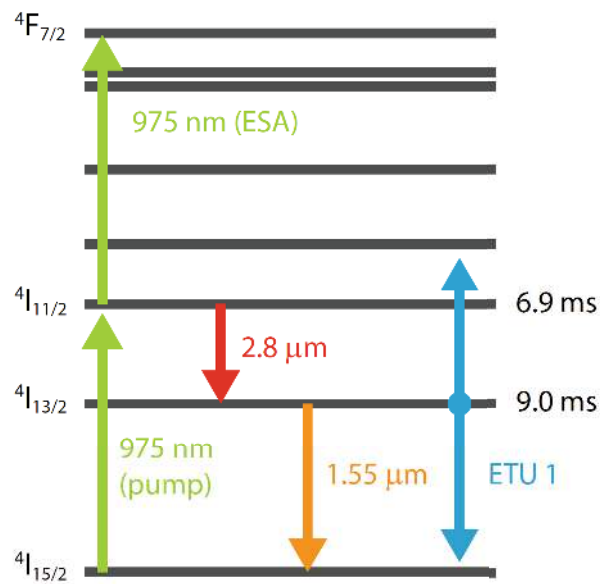


Fig. 3 Schematic of the Er³⁺ ion energy diagram in fluoride fibers. The ground state pumped at 975 nm brings the ions to the upper transition level ${}^4I_{11/2}$ where they radiatively decay to the ${}^4I_{13/2}$ level by emitting a photon around 2.8 μm. While the upper state of the transition is short-lived compared to the lower energy level of the transition, the energy transfer up-conversion process ETU1 avoids the self-termination of the transition by depopulating the ${}^4I_{13/2}$ level and repopulating both the ground state and the upper state of the transition

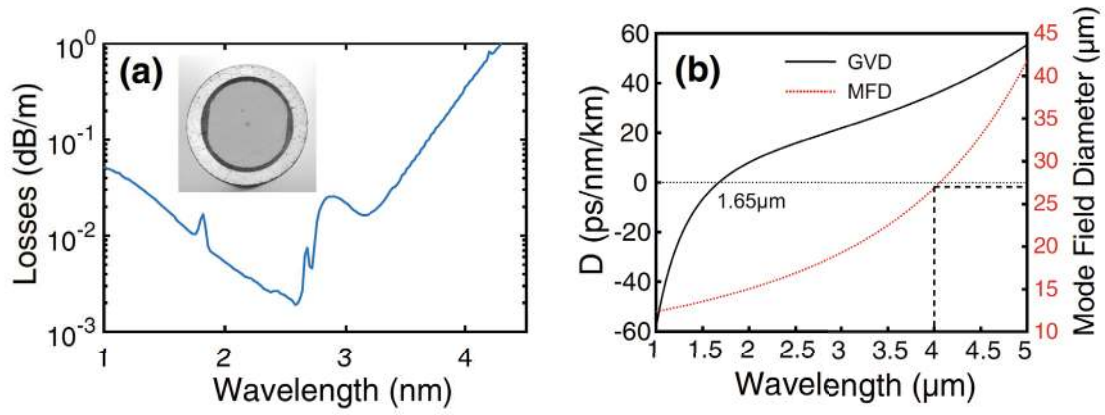


Fig. 4 **a** Losses of the Er-doped fluoride fiber. The double-clad structure and presence of two parallel flats can be seen on the microscope picture (inset). **b** Dispersion (solid black) and LP01 mode field diam-

eter (dashed red) of the Er-doped fluoride fiber. The dispersion was calculated using the Sellmeier equation [26]

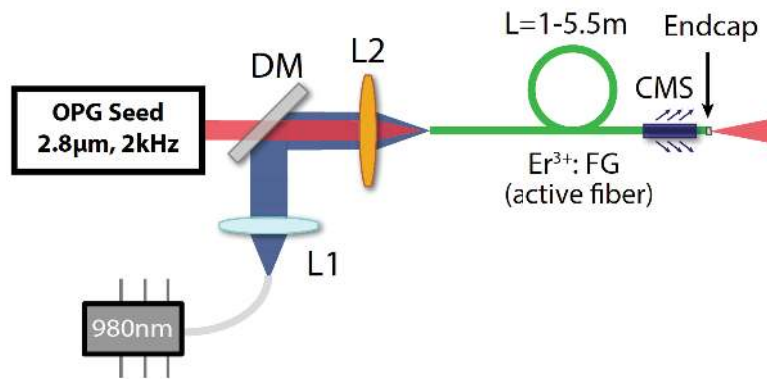
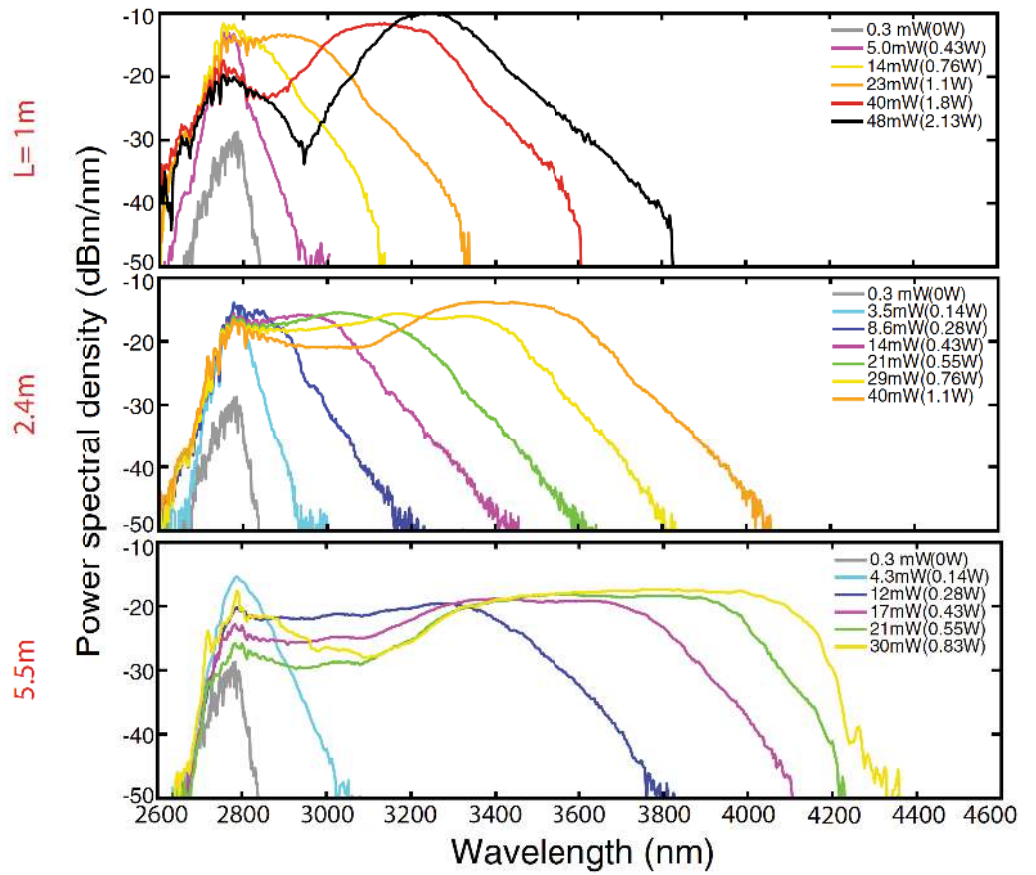


Fig. 5 In-amplifier setup at 2 kHz pumped in co-propagation. A cladding mode stripper (CMS) evacuates the residual pump. The fiber is cleaved at 5° at both ends to prevent parasitic lasing

Fig. 6 Power spectral density of the SC generated with three different amplifier lengths. Each curve's color corresponds to a specific pump power (gray in parenthesis). The SC average output power is shown in black



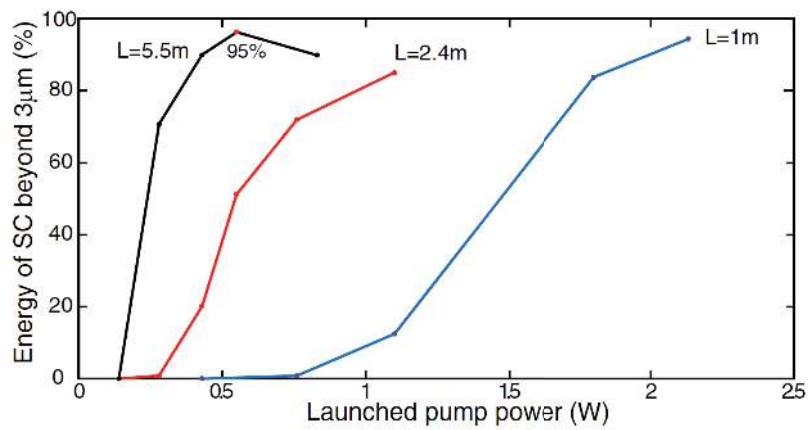


Fig. 7 Fraction of SC energy lying beyond 3 μm increases with pump power for the 3 fiber lengths tested. The maximal energy conversion over 3 μm was 95%, which corresponds to the green curve at 5.5 m presented in Fig. 6

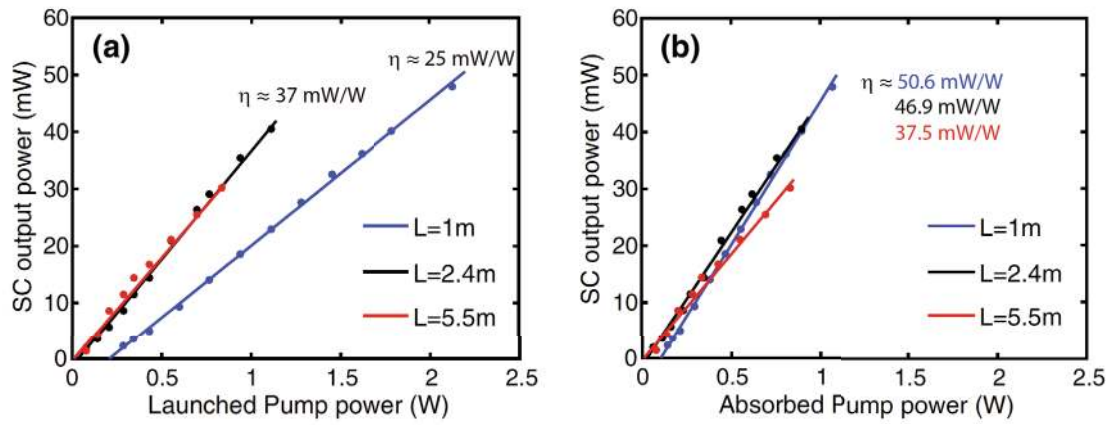


Fig. 8 Amplifying efficiency with respect to **a** launched pumped power and **b** absorbed pump power. The slightly lower efficiency at 5.5 m in **b** is due to the increased background losses when the spectrum reaches wavelengths near $4.2\ \mu\text{m}$

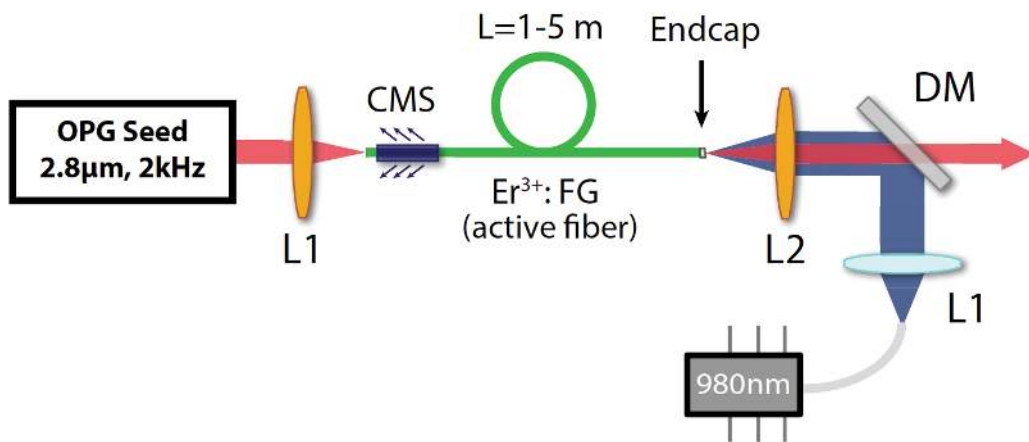


Fig. 9 In-amplifier setup pumped in counter-propagation. Again, the fiber is cleaved at 5° at both ends to delay parasitic lasing. The CMS prevents the residual pump from being sent into the OPG seed

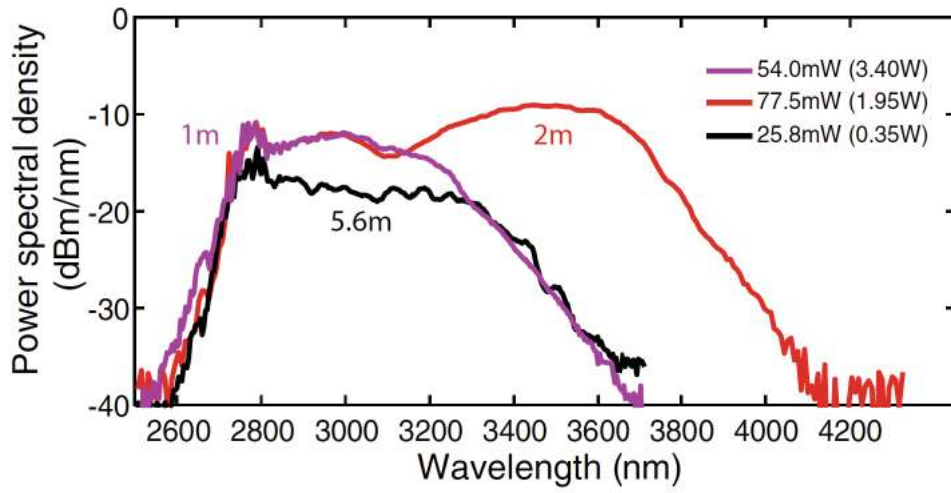


Fig. 10 Best SC obtained with optimized pump power for each tested fiber lengths in counter-propagation at 2 kHz

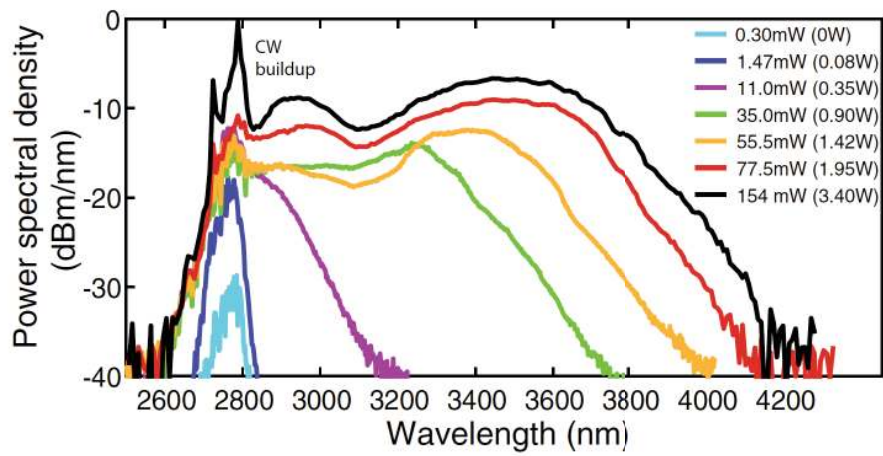


Fig. 11 Spectral evolution of the SC with increasing pump power for the 2 m amplifier pumped in counter-propagation. A buildup of the ASE around 2.8 μm is visible when the pump power becomes sufficiently high, leading to a halt in spectral broadening and the onset of parasitic lasing centered at 2790 nm. More details can be found in [23]

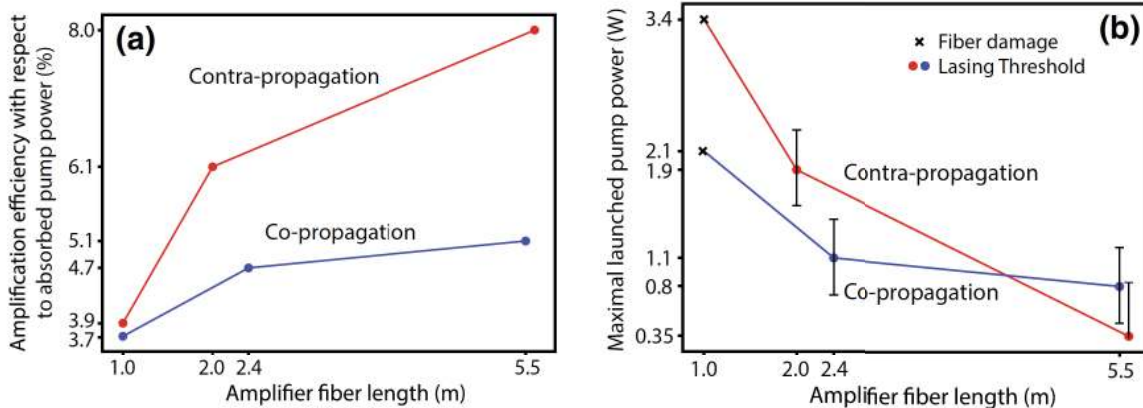


Fig. 12 Comparison of **a** the amplification efficiency and **b** the parasitic lasing threshold for counter and co-propagation pumping depending on fiber length. Because of the availability of the fibers

in the lab, measurements were not taken with the same fiber lengths. Nonetheless, the general trend can be observed from these experiments

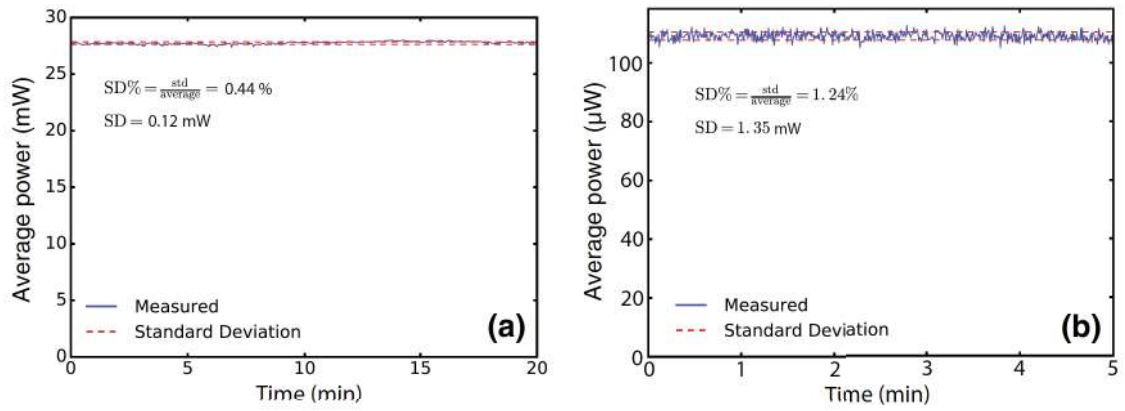


Fig. 13 Average output power variation for **a** the full spectral range and **b** for a 10 nm band around 3500 nm

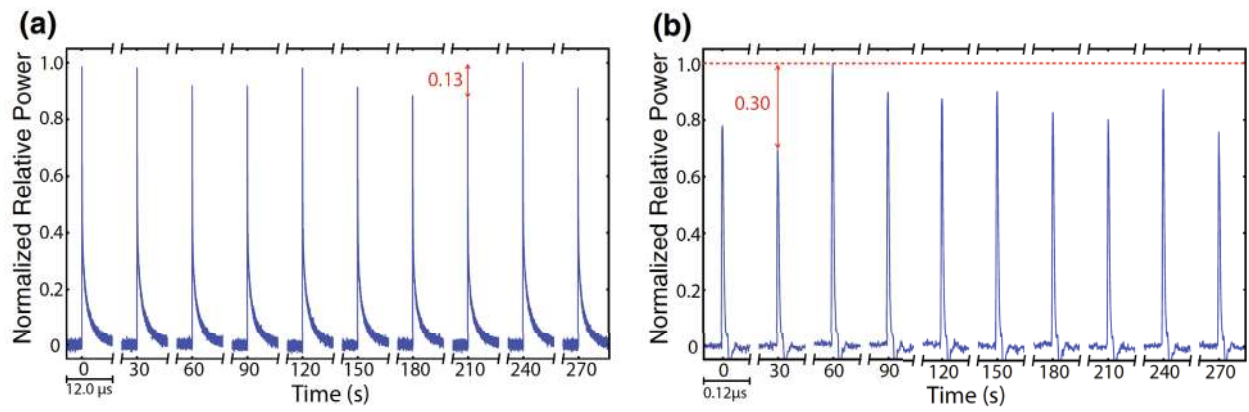


Fig. 14 Pulse-to-pulse variation in time of the power measured with **a** an InSb fast detector (rise time: 100 ns) and **b** an HgCdTe fast detector (rise time: 1 ns)

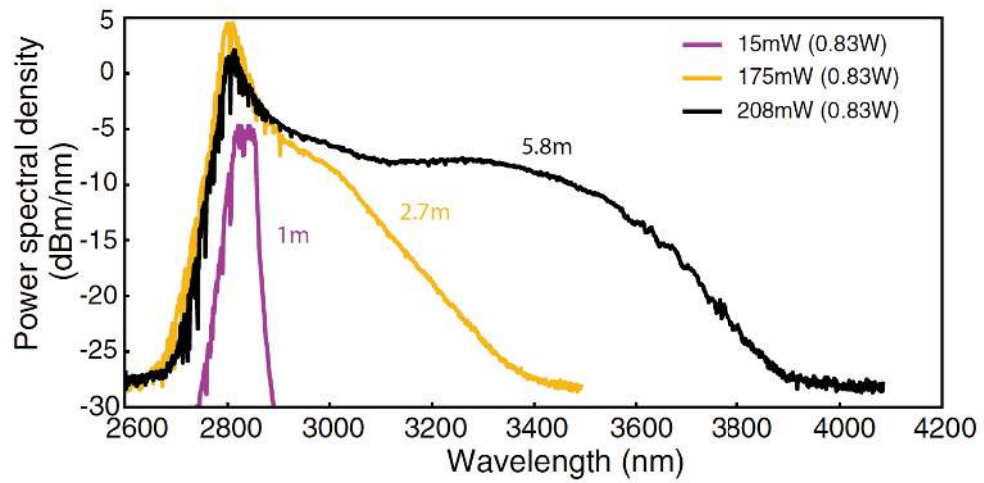


Fig. 15 SC obtained for 1, 2.7 and 5.8 m amplifier lengths with 3 mW of injected seed power at 20 kHz and a pump power of 0.83 W at 976 nm. The effect of fiber length on the SC spectra can be clearly observed here since the spectra were taken under the same pumping conditions

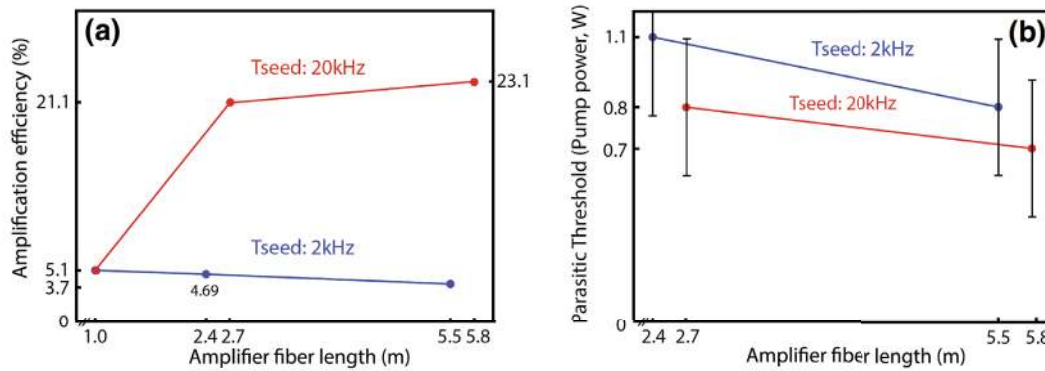


Fig. 16 Comparison of **a** the amplification efficiency and **b** parasitic threshold using the 2 kHz or the 20 kHz seeded amplifiers. The amplification efficiency is calculated with respect to absorbed pump

power to allow comparison between slightly different fiber lengths. The 20 kHz OPG seed launched power was 3 mW (vs 0.3 mW at 2 kHz)

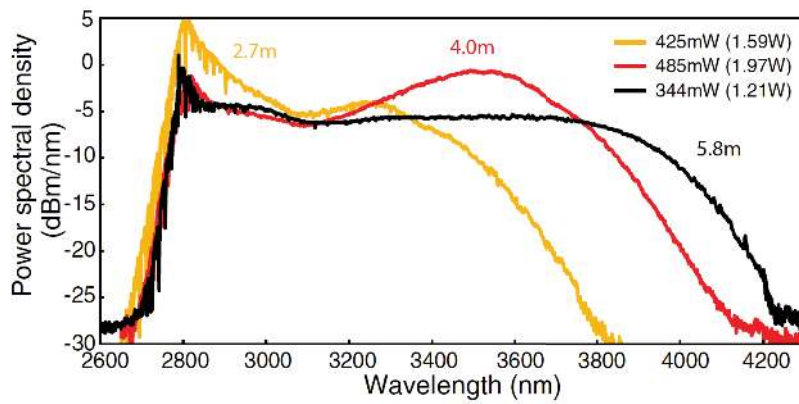


Fig. 17 Spectra with the highest output power achieved with the 20 kHz OPG seed. For the experiment, we also tested a 4 m amplifier to get an intermediate length between 2.7 and 5.8 m, which gave the highest output power. All curves were seeded with 10 mW at 2.8 μm from the OPG source

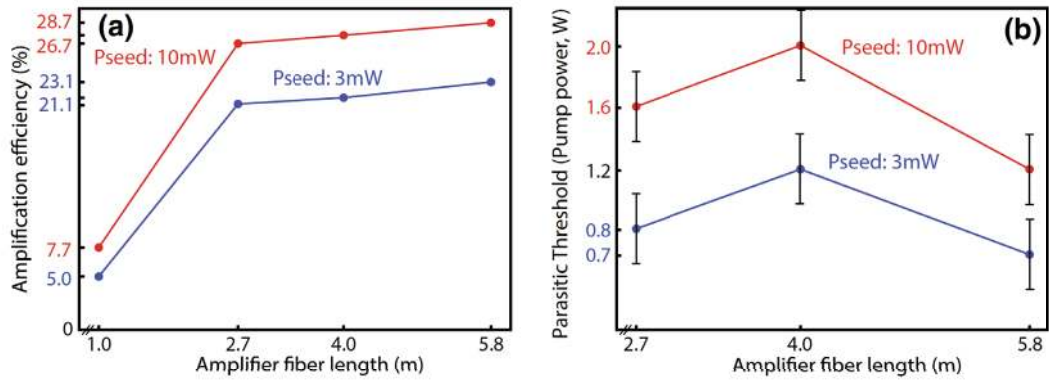


Fig. 18 Comparison of **a** the amplification efficiency and **b** parasitic lasing threshold at OPG seed powers of 3 mW versus 10 mW. The amplification efficiency is calculated with respect to launched pump power

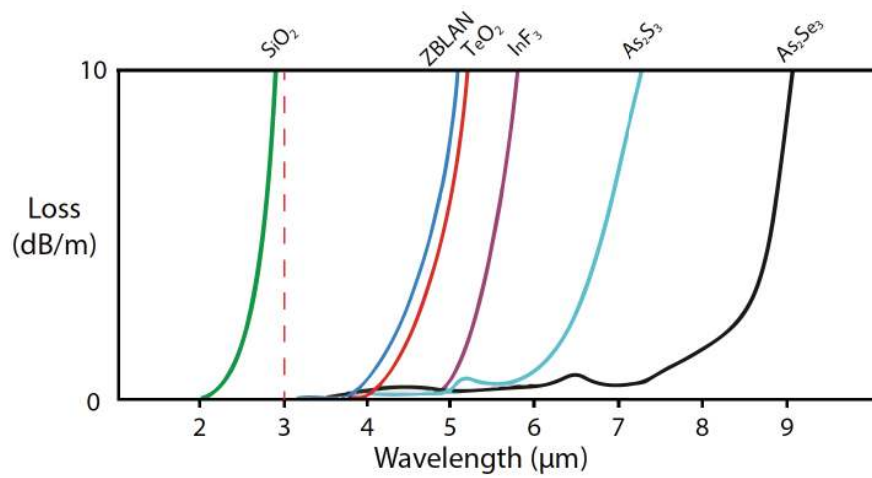


Fig. 19 Transparency of different fibers commonly used in the mid-infrared. Fluoroindate (InF_3) was chosen over other types of fiber due to its commercial availability, relatively low background losses and fusion splicing possibility with ZrF_4 fibers. Adapted from [22]

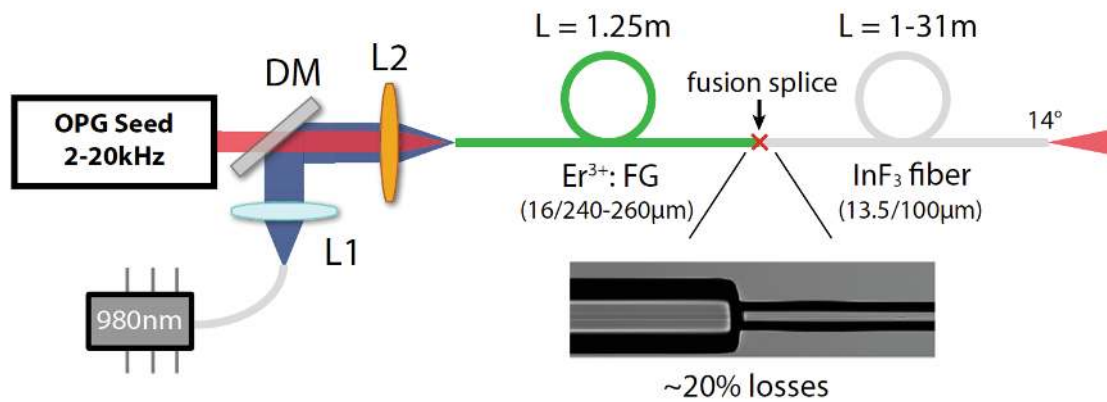


Fig. 20 In-amplifier setup for the InF₃ experiments. A fusion splice (picture) with ~20% losses was realized between the two fibers to improve the robustness of the setup. Since the InF₃ fiber is single-clad, no CMS was needed to evacuate the residual pump power. The fiber output was cleaved at 14° to prevent parasitic lasing

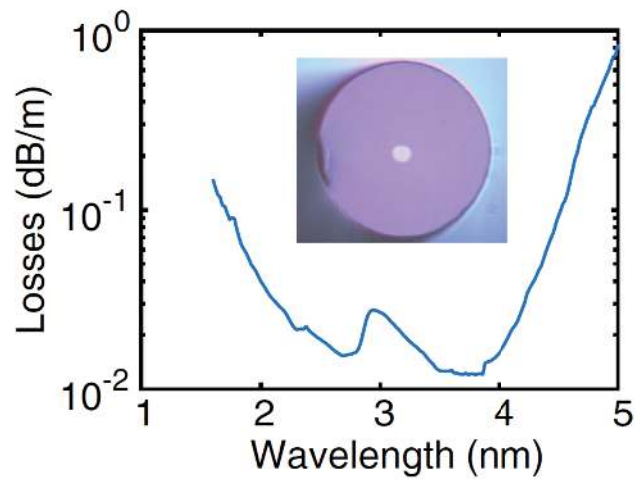


Fig. 21 Microscope image (inset) and attenuation curve of the 12.5/14.5 $\mu\text{m}/100 \mu\text{m}$ InF_3 fiber spliced to the 1.25 m Er: FG fiber amplifier

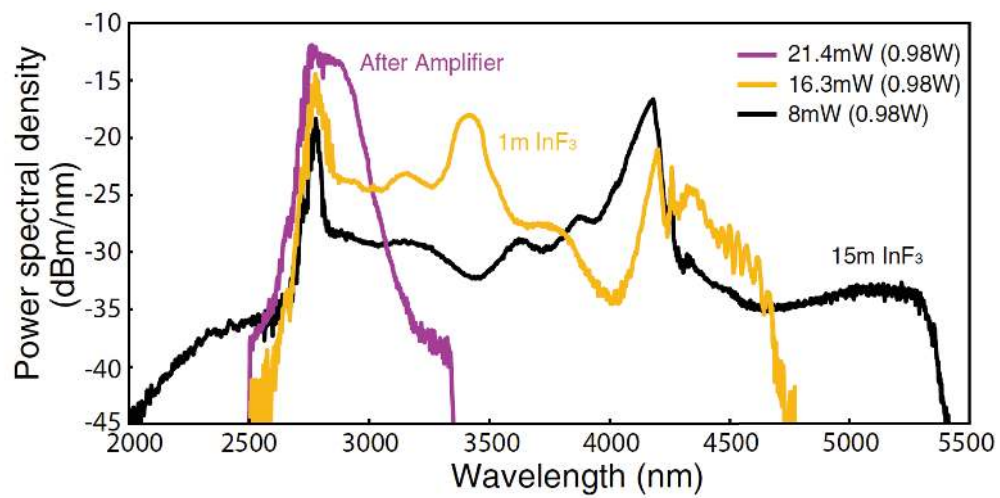


Fig. 22 Spectral evolution of the SC after the 1.25 m Er^{3+} : FG fiber amplifier, 1 m of InF_3 and 15 m of InF_3 fiber. The SC spectrum becomes limited by the edge of the InF_3 fiber transparency window around 5.5 μm

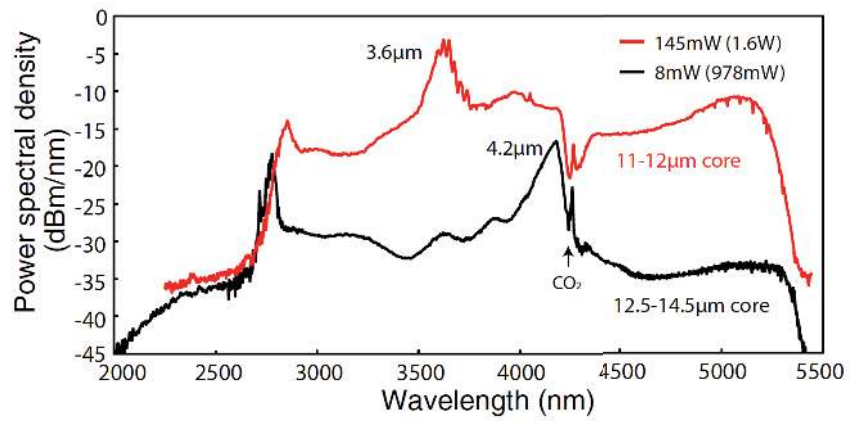


Fig. 23 Best SC spectra measured in InF₃ fibers with core sizes of 11–12 µm (red) and 12.5–14.5 µm (black). The red curve has a higher output power since it was tested with the 20 kHz seed instead of the 2 kHz one (pump power in parenthesis). The prominent peak near 4.2 µm (black) was shifted to 3.6 µm (red) following the core size reduction

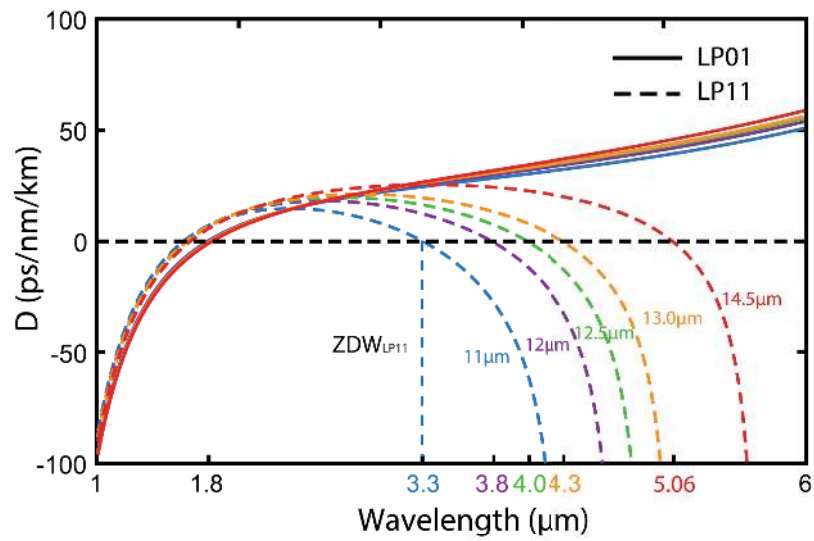


Fig. 24 Simulation of the dispersion curve for the LP01 (solid) and LP11 (dashed) modes based on the Sellmeier coefficients of our InF_3 fibers [26]. While the fundamental mode only exhibits a single ZDW near $1.8 \mu\text{m}$, the LP11 mode have a second ZDW whose value, indicated on the x -axis, changes appreciably depending on the core size (written values)